EEET ECOLOGICAL ENGINEERING & ENVIRONMENTAL TECHNOLOGY

Ecological Engineering & Environmental Technology, 2026, 27(6), 374–391
https://doi.org/10.12912/27197050/221826
ISSN 2719–7050, License CC-BY 4.0

Received: 2026.04.21
Accepted: 2026.05.18
Published: 2026.06.01

Morphology-based baseline assessment of microplastic contamination in the coastal waters of Nouakchott (Mauritania): Spatial structure, seasonal variability, and putative source patterns

Khadijetou El Hacen[1*], Oumar Rouan Hacene[2], Sidi Ahmed Elemin[1], Zeinebou Sidoumou[1]

[1] EBIOME Research Unit, Department of Biology, Faculty of Science and Technology, University of Nouakchott, Mauritania
[2] Department of Biology, University of Oran, 1 Ahmed Ben Bella, 31000 Oran, Algeria
* Corresponding author's e-mail: khatounahassen@gmail.com

ABSTRACT

Microplastic (MP) pollution is a growing threat to West African coastal ecosystems, but Mauritania has no quantitative data to date. We present the first characterization of MP contamination in Nouakchott's coastal surface waters, sampling three sites with contrasting anthropogenic pressures Lwerf (port area), Hotel Sabah (urban tourism zone), and Fish Market (artisanal fishing hub) during the warm and cold seasons. In total, 237 particles were collected using plankton nets (20 µm mesh), examined under a stereomicroscope, and classified by size (small MPs, large MPs, mesoplastics, macroplastics), morphology (filament, fiber, film, fragment), shape, color, and length (0.1–125 mm). Non-parametric tests (Kruskal-Wallis, H = 54.16 – 67.95, $p < 0.001$; Mann-Whitney U, r = 0.535), chi-square/Fisher exact tests with Cramér's V (0.119–0.525), Spearman correlations, PERMANOVA (R^2_{site} = 0.400; R^2_{season} = 0.399; combined = 79.9%), PCA, and correspondence analysis (CA) were applied. Together, site and season accounted for roughly 80% of multivariate variance in MP composition. Season had the strongest effect on particle size (η^2_H = 0.282): cold-season samples were dominated by mesoplastics and macroplastics, while the warm season brought smaller particles. CA uncovered site-specific morphological signatures fibers at Hotel Sabah (morphologically compatible with domestic effluents), films at Fish Market (compatible with single-use packaging), filaments at Lwerf (compatible with fishing-gear materials). Shannon color diversity confirmed Lwerf as the most heterogeneous site (H' = 1.814, 95% CI [1.36–1.99]), pointing to contamination from multiple sources. These results establish a first morphology-based baseline for MP monitoring in Mauritania and call for management strategies tailored to each site and season. Source attributions are presented as hypotheses requiring polymer-level (FTIR/Raman) verification in future work.

Keywords: microplastics, Nouakchott, Mauritania, West Africa, coastal pollution, PERMANOVA, seasonal variation, correspondence analysis.

INTRODUCTION

Microplastics (MPs), defined as synthetic polymer particles below 5 mm (Thompson et al., 2004), now rank among the most widespread contaminants of the marine environment (Andrady, 2011; GESAMP, 2015). Global plastic production surpassed 400 million tonnes in 2023 (PlasticsEurope, 2024), and between 8 and 12 million tonnes reach the ocean each year (Jambeck et al., 2015), of which a substantial share enters the marine environment as primary microplastics released directly from textiles, tyres and personal-care products (Boucher and Friot, 2017). MPs turn up everywhere from polar snow (Bergmann et al., 2019) to deep-sea sediments (Woodall et al., 2014). Because they resist biodegradation, adsorb persistent organic pollutants, and are ingested across trophic levels, they pose linked ecological and public-health risks (Cole et al., 2011; Rochman et al.,

2019). Their global accumulation on shorelines worldwide, fed by both primary inputs and secondary fragmentation, has been documented since Browne et al. (2011). Two decades after Thompson et al. (2004) first raised the alarm, a retrospective in Science concluded that research has shifted from documenting MP occurrence toward understanding particle-specific hazards and environmental fate (Thompson et al., 2024).

Coastal zones sit at the receiving end of terrestrial runoff, river discharge, atmospheric deposition, and direct human inputs, making them particularly exposed (Lebreton et al., 2017; Bao et al., 2023). Within these transitional environments, MP abundance and characteristics depend on interactions among pollution sources, hydrodynamic conditions, and seasonal factors temperature, UV intensity, biological activity (Li et al., 2018; Isobe et al., 2019). Seasonal effects can be substantial: winter conditions generally favor larger particles owing to slower photodegradation and greater stormwater transport (Enders et al., 2015; Prata et al., 2019). In a Brazilian tropical estuary, Silva Barbosa et al. (2025) recently showed that season reshapes MP shape and color composition even when total particle counts stay constant. Despite such observations, studies that deploy multivariate frameworks PERMANOVA, correspondence analysis, diversity indices to separate spatial from temporal drivers remain scarce, especially in developing countries (Chukwuka et al., 2024).

West Africa bears a disproportionate share of plastic pollution. The region produced 6.9 million tonnes of plastic waste in 2018, with 20% generated within 30 km of the coast (World Bank, 2023). Coastal MP concentrations off Ghana reach 1,000 particles/m³ (Aragaw, 2021), and contamination has been found in over 80% of sampled marine species in Nigeria (Alimi et al., 2021). Riverine inputs add up to 500 particles/L in the Niger Delta. Chukwuka et al. (2024) built vulnerability indices for West African coastlines from remote-sensed oceanographic data, but ground-truth field measurements remain sparse. Around Dakar, Sonko et al. (2023) confirmed that proximity to wastewater outfalls drives both MP and microbiological contamination. Mauritania, however, has produced no MP data at all -an important blind spot given that its waters support some of Africa's most productive fisheries (Okeke et al., 2022).

Mauritania's Atlantic coast stretches roughly 750 km and sustains major artisanal and industrial fisheries, with Nouakchott serving as both capital and fast-growing urban center. Plastic accounts for about 9% of the city's municipal solid waste (Mint Sidi Mohamed, 2017), and without modern treatment infrastructure, leakage into the coastal zone is substantial. The Canary Current upwelling system introduces a strong oceanographic signal during the cold season, potentially influencing the transport and accumulation of floating debris (Valdés and Déniz-González, 2015). Abandoned, lost, or discarded fishing gear (ALDFG) is a growing contributor to marine plastic pollution worldwide (Richardson et al., 2019; Gilman et al., 2021), and the intensive fisheries off Mauritania make this pathway particularly relevant. Yet no quantitative MP baseline exists for any Mauritanian water body.

The present work fills that gap. We sampled three coastal sites in Nouakchott — Lwerf (port area), Hotel Sabah (urban tourism zone), and Fish Market (artisanal fishing hub) — during both the warm and cold seasons, with four objectives: (i) quantify and describe MP morphological characteristics (length, type, morphology, shape, color) by site and season; (ii) test for significant compositional differences using non-parametric tests; (iii) characterize the multivariate structure of MP assemblages through PERMANOVA, PCA, and correspondence analysis; and (iv) evaluate assemblage diversity and evenness with Shannon indices to infer source heterogeneity.

MATERIALS AND METHODS

Study area

Sampling took place along Nouakchott's Atlantic coast (17°56'–18°10' N). Three sites were chosen for their contrasting anthropogenic profiles (Figure 1): (1) Lwerf (Warf), a port area with moderate population density and mixed residential-commercial activity, geo-referenced at 18°06'09" N, 16°01'40" W; (2) Hotel Sabah, a coastal tourism zone with seasonal hotel and restaurant traffic, located at 18°06'40" N, 16°01'36" W; and (3) Fish Market (Marché au Poisson), an intensive artisanal fish-landing and processing site, located at 18°06'11" N, 16°01'33" W. Each site was geo-referenced in situ; four duplicate stations (AN1–AN4) were set up along the shoreline at each site, distributed along four transects of 100 m each. Detailed station-level GPS coordinates, GIS shapefiles of all sampling locations,

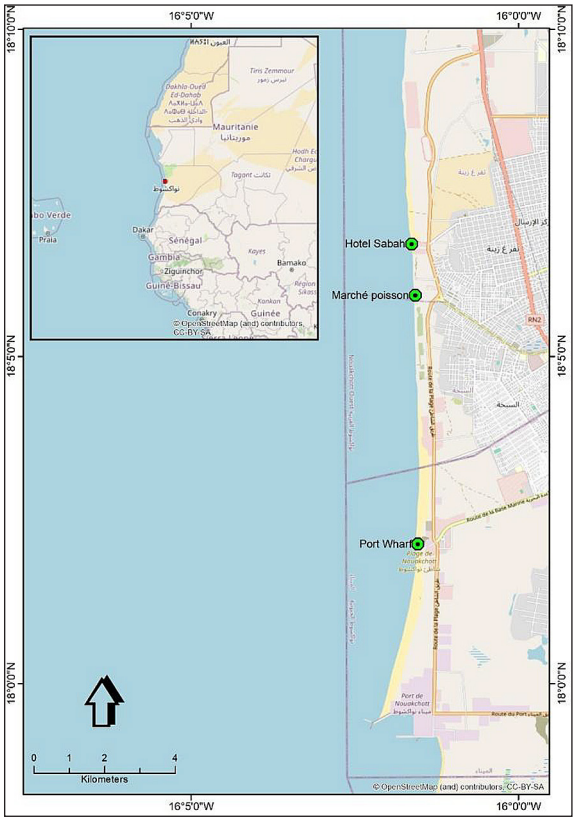

Figure 1. Map of the study area showing the location of the three sampling sites along the coast of Nouakchott (Mauritania): Lwerf (port area), Hotel Sabah (urban tourism zone), and Fish Market (artisanal fishing hub)

and time-stamped field photographs of every sampling event are provided as Supplementary Materials (Annex S1).

Sampling protocol

The sampling methodology adopted in this study follows the protocol of Prata et al. (2019) for surface-water microplastic collection, with minor adaptations to local field conditions. Two seasonal campaigns were carried out: a warm-season campaign on 01–03 September 2024, and a cold-season campaign on 01–03 December 2024. The exact sampling schedule was as follows: warm season — Port Wharf (Lwerf) on 01-09-2024 at 15:40, Hotel Sabah on 02-09-2024 at 16:10, and Fish Market on 03-09-2024 at 16:40; cold season — Port Wharf on 01-12-2024 at 13:40, Hotel Sabah on 02-12-2024 at 14:10, and Fish Market on 03-12-2024 at 14:40. At each site and during each campaign, four samples were collected from four distinct transects of 100 m each (replicates AN1–AN4), giving a total of 24 surface-water samples across the two campaigns.

Surface water was sampled using a plankton microfiltration net (reference SOC-C1037305) with a 20 µm mesh aperture made of technical nylon (Nitex-type), conical in shape, fitted on a galvanized steel ring of 200 mm diameter and equipped with a 100 mL polyethylene collection vessel at the cod-end. The net was deployed and towed at approximately 15 cm depth along each 100 m transect. Pre-numbered glass containers and a Formica board with marker were used in situ to label and code each sample. The net contents were rinsed into pre-cleaned glass jars with distilled water; all samples were stored in glass containers and transported to the laboratory, where they were refrigerated and processed within 24 h. The two campaigns covered the warm season (sea-surface temperature > 28 °C, coinciding with peak tourism and fishing) and the cold season (SST < 25 °C, associated with coastal upwelling). The complete net specifications datasheet, raw field sampling logs (date, time, GPS coordinates, chain-of-custody documentation from field to laboratory, and time-stamped field photographs of every sampling event at all three sites are provided as supplementary materials.

Environmental metadata were recorded at each station during each sampling event, including water depth, distance from shore, tidal state, water temperature, wind speed and direction, salinity, pH, dissolved oxygen, conductivity and total dissolved solids (Tables S1 and S2). Water depth was consistently between 0.1 and 0.5 m, and all samplings were conducted at mid-tide. During the warm-season campaign, water temperature averaged 28–29 °C, salinity was 35.2 PSU, pH was 7.8, dissolved oxygen ranged from 5.65 to 6.90 mg/L, conductivity was 56.9 mS/cm, TDS reached 55 g/L, and winds were light (0.8 m/s) from the southwest. During the cold-season campaign, water temperature dropped to 24 °C, salinity rose slightly to 36 PSU, pH ranged from 7.70 to 8.16, dissolved oxygen increased to 7.70–7.90 mg/L (consistent with cooler, upwelling-influenced waters), conductivity was 54–54.2 mS/cm, TDS was 55.0–55.4 g/L, and winds strengthened to 4.4 m/s from the northeast. The full station-level environmental dataset is reproduced in Tables S1 and S2 (supplementary materials – Annex S2) together with raw field measurement sheets.

The volume of water filtered per tow was estimated geometrically from the net specifications: with a circular ring opening of 200 mm diameter (cross-sectional area ≈ 0.0314 m²) and a horizontal towing distance of 100 m, each tow filtered approximately 3.14 m³ of surface water, for a total filtered volume of ≈ 75 m³ across the 24 tows. Because a calibrated flow-meter was not available, this volume is reported as a geometric estimate rather than a measured value, and we therefore present the dataset in terms of comparative compositional patterns (counts, proportions, multivariate structure) rather than as absolute particle concentrations (particles/m³). The 20 µm mesh aperture was selected to maximise the capture of the smallest microplastic fraction (S MPs < 1 mm), which is poorly retained by the 300–333 µm mesh sizes commonly used in marine MP surveys (Prata et al., 2019); we acknowledge however that a fine mesh of this aperture also increases the risk of co-collection of airborne and procedural particles, which is why the quality-control protocol included paired laboratory and procedural blanks for every sampling batch (Figure 2).

All samples were refrigerated upon return to the laboratory before being sorted, treated and analysed. Laboratory processing required the following equipment: glass Petri dishes, glass beakers, metal forceps, distilled water, 70% ethanol, and a binocular stereomicroscope. Samples were first deposited on flat-surface receptacles. Coarse organic debris and planktonic organisms were carefully removed with forceps and placed in a crystallizer; each removed object was rinsed with distilled water to detach any adhering microplastic particles, which were recovered and added back to the sample. The cleaned samples were then transferred in small aliquots into glass beakers and a small volume of 70% ethanol was added. Following Prata et al. (2019), 70% ethanol serves a dual purpose: it preserves the sample, and during visual inspection it decolorizes residual organic matter, making colored plastic particles substantially easier to detect.

Sample analysis was performed under a binocular stereomicroscope (×10–×40) and, when needed, complemented with an optical microscope, both fitted with calibrated measurement reticles. Particles sorted from each net replicate were transferred into pre-coded glass Petri dishes. To prevent particle loss, all containers were rinsed thoroughly so that any particle adhering to the glass walls was washed back into the Petri dish. Each retained particle was classified by: (i) type -small MPs (S MPs, < 1 mm), large MPs (L MPs, 1–5 mm), mesoplastics (MESO, 5–25 mm), macroplastics (MACRO, > 25 mm), following GESAMP (2015); (ii) morphology – filament, fiber, film, or fragment; (iii) shape – regular or irregular; (iv) color – recorded visually; and (v) length – measured with a calibrated digital caliper (mm) under the stereomicroscope. All information (item number, shape, length, color, polymer aspect) was recorded on individual classification sheets to feed the statistical study. The full set of raw laboratory bench sheets, the unprocessed stereomicroscope observation logs (particle-by-particle records before classification), the high-resolution microscope image archive of every particle (with scale bars), the calibration records for the stereomicroscope and digital caliper, the complete particle inventory dataset (raw attributes before any filtering), the data exclusion and cleaning log, the documentation of GESAMP classification decision rules applied in practice, and photographic evidence of the laboratory workflow (contamination-control conditions, blanks where applicable) are provided as supplementary materials (Annex S3). Because polymer identification techniques such as FTIR or Raman spectroscopy were not available during the present study, particle identification relied exclusively on morphological criteria under stereomicroscopy. To reduce the risk of false-positive identification, only particles meeting established visual criteria (absence of cellular structure, homogeneous coloration, synthetic appearance, and resistance to manipulation) were retained, following recommendations from Prata et al. (2019) and Hartmann et al. (2019). The resulting dataset should therefore be considered a morphology-based baseline assessment rather than a chemically validated polymer inventory. Particles indistinguishable from blank-type fibres or fragments were nevertheless flagged in the raw classification sheet (Annex S3) so that any subsequent re-analysis can apply a more conservative subtraction if needed. Morphological identification was retained as the sole identification method in this first baseline for three converging reasons: (i) FTIR and Raman spectrometers were not accessible at the national laboratory infrastructure available to the project at the time of the campaigns; (ii) the primary objective was to establish a first comparative description of the contamination pattern across

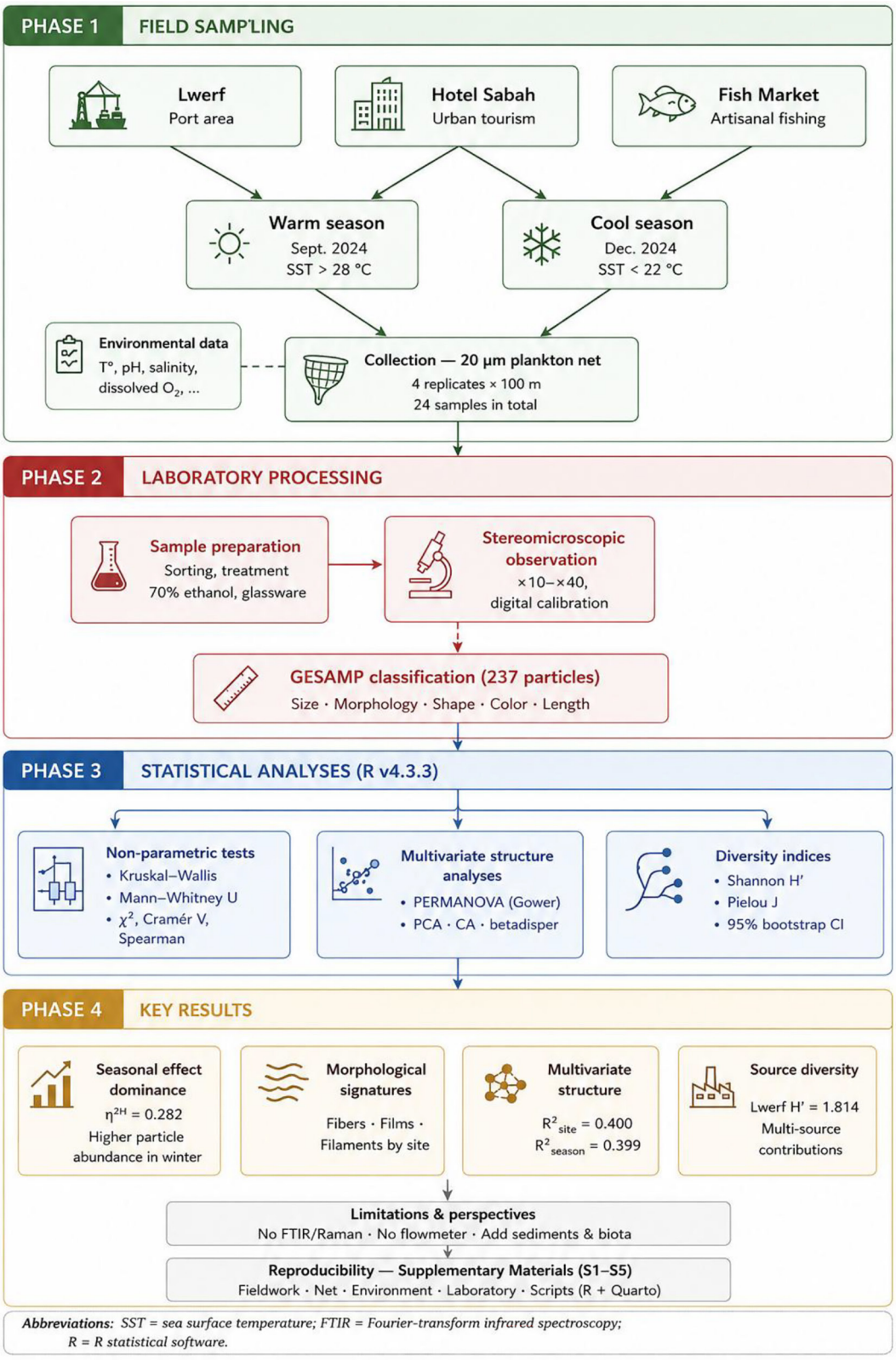

Figure 2. Workflow of the microplastic baseline assessment carried out on Nouakchott's coastal waters

sites and seasons (proportions, multivariate composition, diversity), for which morphological categorisation is a valid and widely-used first step in the West-African and tropical-coastal MP literature (Aragaw, 2021; Sonko et al., 2023; Chukwuka et al., 2024); and (iii) every classification decision was made under standardised visual criteria (Hartmann et al., 2019) and is supported by a raw image archive (Annex S3) that allows independent re-examination – and,

in future work, re-analysis by FTIR/Raman on the retained subset. We therefore explicitly acknowledge that all polymer-type and source attributions presented hereafter are morphological hypotheses, not chemically validated identifications. All methodological evidence – raw laboratory bench sheets, unprocessed stereomicroscope observation logs (particle by particle, before classification), is available in Annex S3.

Statistical analyses

All analyses were run in R v.4.3.3. Normality was assessed with Shapiro-Wilk tests, variance homogeneity with Levene's test. Because parametric assumptions were systematically violated, we adopted the following non-parametric framework:

1. Kruskal-Wallis tests for length differences among sites and seasons, with Dunn's post-hoc comparisons (Bonferroni correction); Mann-Whitney U for two-group seasonal contrasts. Effect sizes: η^2_H and r (Cohen, 1988).
2. Chi-square tests (Fisher's exact when expected counts < 5) for associations between categorical variables (type, morphology, shape, color) and site or season. Cramér's V measured association strength (Cramér, 1946).
3. Spearman rank correlations for all variable pairs ($\alpha = 0.05$).
4. PERMANOVA (adonis2, 999 permutations, Gower distance) for multivariate compositional differences, with betadisper for dispersion homogeneity (Anderson, 2017).
5. PCA (FactoMineR) and correspondence analysis (CA) for ordination and site–variable associations.
6. Shannon diversity (H') and Pielou evenness (J) per site × season cell (Shannon, 1948).

Significance threshold: $\alpha = 0.05$. Packages: car, FSA, rstatix, effectsize, vcd, vegan, FactoMineR, ggplot2, corrplot.

To support full reproducibility of the analysis, the complete set of analytical resources is provided as supplementary materials (Annex S4): the R scripts (.R files) used for all statistical tests and figure generation; the R session information (package versions, dependencies and system environment); the raw output files for every test performed (Kruskal-Wallis, Dunn, Mann-Whitney, Chi-square, Fisher exact, PERMANOVA); the permutation and distance (Gower) matrices used in PERMANOVA; the input matrices and full eigenvalue outputs for the PCA and correspondence analyses; the replication-structure file mapping the duplicate stations AN1–AN4 to each site and season; and a versioned, fully reproducible analysis workflow as an R Markdown / Quarto report. The complete archive of all plotted figures before publication editing (raw graphical outputs) and a data dictionary defining every variable, coding rule and threshold used in classification are also included in Annex. Because multiple particles were obtained from the same tow samples, some degree of non-independence among observations cannot be excluded. The present analyses therefore describe particle-level patterns within a limited sampling framework (24 tow samples) and should be interpreted cautiously with respect to strict statistical independence. Future studies should incorporate hierarchical or mixed-effects approaches explicitly accounting for nested sampling structure. All methodological evidence underlying Section Statistical analyses – R scripts (.R files), R session information, raw output files for every test performed, permutation and distance (Gower) matrices used in PERMANOVA, input matrices and full eigenvalue outputs of the PCA and CA, replication-structure file mapping the stations AN1–AN4 to each site and season, is available in Annex S4.

RESULTS AND DISCUSSION

Verification of statistical assumptions

Shapiro-Wilk tests rejected normality for the overall length distribution ($W = 0.724$, $p < 0.001$) and for five of six Site × Season subgroups ($p < 0.001$); only Hotel Sabah in the cold season passed ($W = 0.930$, $p = 0.120$). Levene's test confirmed heterogeneous variances across sites ($F = 13.11$, $p < 0.001$), seasons ($F = 37.70$, $p < 0.001$), and their interaction ($F = 9.65$, $p < 0.001$). The right-skewed frequency distributions and departures from the normal reference line visible in Figure 3 left no doubt that non-parametric methods were required throughout.

Descriptive statistics and size distributions

Across the 237 collected particles, lengths spanned three orders of magnitude – from 0.1

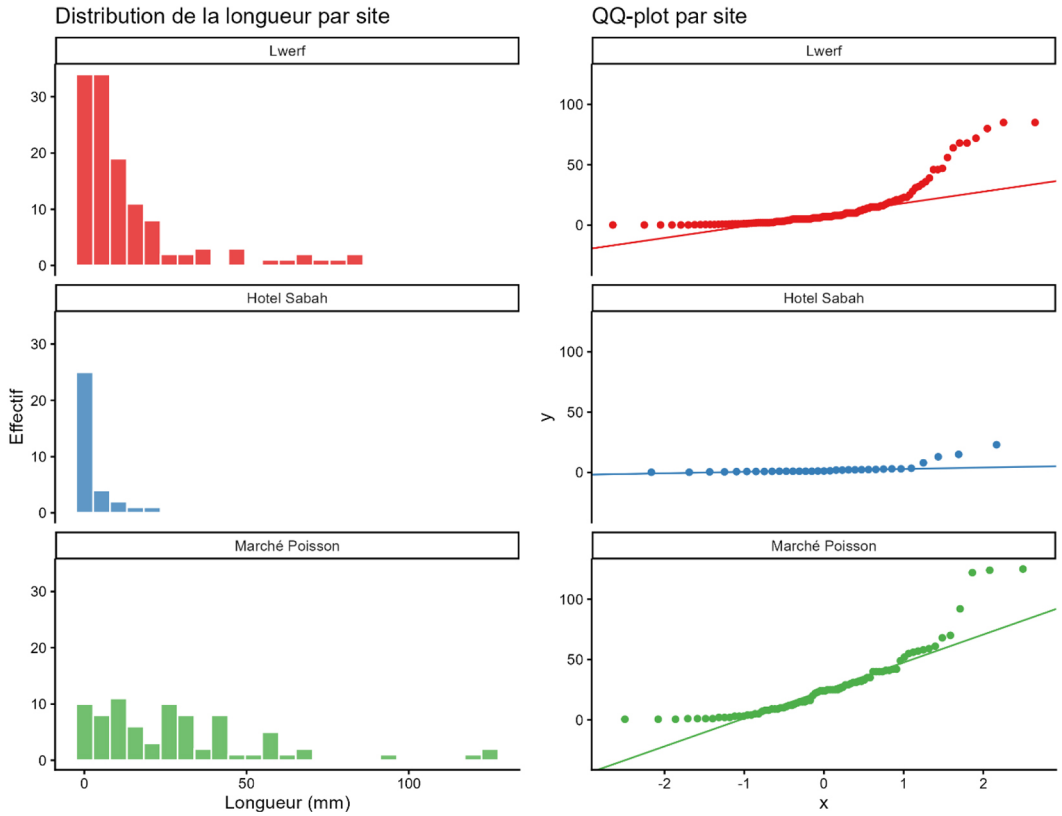

Figure 3. Histograms (left) and QQ plots (right) of MP length for each site. Frequency distributions are right-skewed in all cases. QQ plots show clear departures from the theoretical normal line, particularly at upper quantiles, confirming the non-normal nature of the data

Table 1. Descriptive statistics of MP length (mm) by site and season. N = number of particles; SD = standard deviation; CV% = coefficient of variation; Q1–Q3 = interquartile range. Bootstrap 95% confidence intervals (1,000 iterations, percentile method, package boot) for the subgroup means: Lwerf-Warm [2.02–3.67]; Lwerf-Cold [15.31–24.09]; Hotel Sabah-Warm [2.25–10.37]; Hotel Sabah-Cold [1.22–2.04]; Fish Market-Warm [3.07–8.73]; Fish Market-Cod [30.29–44.07]

Site	Season	N	Mean ± SD	Median	Min–Max	Q1–Q3	CV%
Lwerf	Warm	44	2.79 ± 2.79	2.00	0.1–13.0	0.78–4.18	100.0
Lwerf	Cold	80	19.52 ± 20.85	11.50	0.5–85.0	6.00–22.25	106.8
Hotel Sabah	Warm	11	6.08 ± 7.68	1.00	0.9–23.0	1.00–10.50	126.3
Hotel Sabah	Cold	22	1.60 ± 1.01	1.30	0.2–3.5	0.80–2.38	63.4
Fish Market	Warm	22	5.52 ± 6.99	3.00	0.5–25.0	1.00–7.25	126.5
Fish Market	Cold	58	36.76 ± 27.35	30.50	3.0–125.0	17.00–42.00	74.4

mm to 125.0 mm -with sharp differences among groups (Table 1). Fish Market in the cold season yielded the largest fragments (mean = 36.76 ± 27.35 mm; median = 30.5 mm), whereas Hotel Sabah in the cold season had the smallest (mean = 1.60 ± 1.01 mm). Within-group variability was high everywhere: coefficients of variation ranged from 63% to 127%. The box-and-violin plots in Figure 4 make these contrasts immediately visible. Mesoplastics dominated overall (36.3%), followed by large MPs (30.8%), macroplastics (21.5%), and small MPs (11.4%) – a size profile skewed toward larger fractions, consistent with limited photodegradation and proximity to direct anthropogenic inputs at all three sites.

Seasonal control over particle size

Kruskal-Wallis tests detected highly significant length differences both among sites (H =

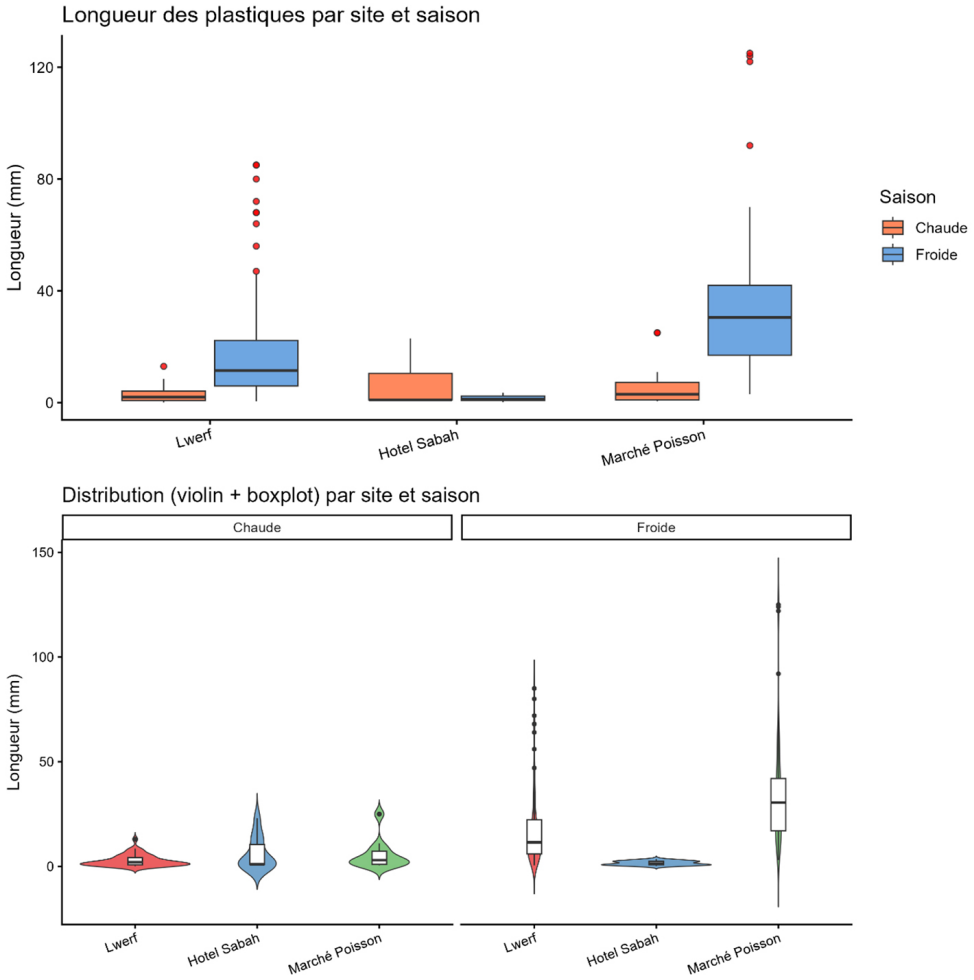

Figure 4. MP length distributions by site and season. Top panels: box plots with outliers shown in red. Bottom panels: violin plots with embedded box plots, illustrating the density profile of each subgroup. Note the order-of-magnitude difference in scale between sites and seasons

54.16, df = 2, $p < 0.001$, $\eta^2_H = 0.223$) and between seasons ($H = 67.95$, df = 1, $p < 0.001$, $\eta^2_H = 0.282$; Table 2). The seasonal effect size exceeded the spatial one, meaning that when and not just where samples were taken matters more for particle size. Mann-Whitney U confirmed a large seasonal effect ($r = 0.535$). Dunn's post-hoc comparisons separated all three site pairs ($p < 0.001$); the widest gap lay between Hotel Sabah and Fish Market ($Z = -7.13$).

The cold-season dominance of larger particles (MESO, MACRO) fits the pattern described by Enders et al. (2015) and confirmed in the Mediterranean (Fossi et al., 2023) and East Asian seas (Isobe et al., 2019). One possible explanation is that reduced photo-oxidative fragmentation and altered hydrodynamic transport during the cold season may favor the persistence and redistribution of larger particles, although these mechanisms were not directly measured in the present study. Silva Barbosa et al. (2025) observed a similar phenomenon in a Brazilian estuary, where seasonal hydrodynamic shifts reshaped MP morphological composition without altering total counts. Taken together, these comparisons reinforce the idea that season modifies MP quality (size, shape) more than quantity. One exception deserves attention. At Hotel Sabah, warm-season particles were unexpectedly larger (mean = 6.08 mm) than cold-season ones (mean = 1.60 mm) — the opposite of the general trend. The most plausible explanation is that summer tourism generates episodic inputs of intermediate-size plastics (food wrappers, beverage containers) that enter the water directly, bypassing the background fragmentation cycle. Pappoe et al. (2022) reported a comparable source-driven anomaly near Ghanaian beach resorts, where tourist-activity peaks introduced distinct particle profiles regardless of seasonal degradation patterns.

Table 2. Non-parametric tests comparing MP lengths across sites and seasons. η^2H = Kruskal-Wallis effect size (> 0.14 = large); r = Mann-Whitney effect size (> 0.5 = large). *** p < 0.001

Test	Factor / Pair	Statistic	df	p-value	Sig.	Effect size	Interpret.
Kruskal-Wallis	Site	H = 54.16	2	< 0.001	***	η^2H = 0.223	Large
Kruskal-Wallis	Season	H = 67.95	1	< 0.001	***	η^2H = 0.282	Large
Mann-Whitney U	Season	W = 2,087	—	< 0.001	***	r = 0.535	Large
Dunn (Bonf.)	Lwerf vs. Hotel Sabah	Z = −4.13	—	< 0.001	***	—	—
Dunn (Bonf.)	Lwerf vs. Fish Market	Z = −4.65	—	< 0.001	***	—	—
Dunn (Bonf.)	Hotel Sabah vs. Fish Mkt	Z = −7.13	—	< 0.001	***	—	—

Table 3. Chi-square tests, Fisher exact tests, and Cramér's V for associations between categorical MP variables and site or season. V < 0.1 = negligible; 0.1–0.3 = weak; 0.3–0.5 = moderate; > 0.5 = strong

Var. 1	Var. 2	χ^2	df	p (χ^2)	p (Fisher)	Sig.	Cramér V	Strength
Type	Site	59.31	6	< 0.001	0.0001	***	0.354	Moderate
Type	Season	65.40	3	< 0.001	—	***	0.525	Strong
Morphol.	Site	26.11	6	< 0.001	0.0001	***	0.235	Weak
Morphol.	Season	3.38	3	0.336	0.311	ns	0.119	Weak
Shape	Site	7.70	2	0.021	—	*	0.180	Weak
Shape	Season	7.59	1	0.006	—	**	0.189	Weak

Note: *** p < 0.001, ** p < 0.01, * p < 0.05, ns = not significant.

Categorical composition and association strength

Type × Season yielded the strongest categorical association in our dataset (χ^2 = 65.40, df = 3, p < 0.001, Cramér's V = 0.525, "strong"), followed by Type × Site (χ^2 = 59.31, V = 0.354, "moderate") and Morphology × Site (χ^2 = 26.11, V = 0.235, "weak"; Table 3). Morphology showed no significant link with season (p = 0.336). However, the absence of statistical significance should not be interpreted as evidence of true seasonal stability in particle morphology. Given the relatively limited sampling effort, this result may also reflect reduced statistical power to detect subtle seasonal effects. Figure 5 displays the proportional breakdowns by type, morphology, and color. Blue and transparent particles dominated across all sites and visually resembled packaging-related plastics commonly reported in coastal environments, although polymer composition was not chemically confirmed.

Pairing Cramér's V with chi-square tests – as recommended by Hartmann et al. (2019) for MP research but seldom done in practice -lets us go beyond binary reject/accept decisions and compare association strengths on the same scale. The strong V for type × season (0.525) versus the weak V for morphology × season (0.119) puts a number on what the raw counts already suggest: season reshapes the size spectrum far more than it alters morphological makeup.

Spearman correlations

Length and type were almost perfectly correlated (ρ = 0.955, p < 0.001). This very high correlation is expected because the size-type categories (S MPs, L MPs, MESO, MACRO) were themselves defined using particle-length thresholds. The relationship is therefore structural by construction and should not be interpreted as an independent ecological association. Rather than validating the biological meaning of the classification, this result simply confirms the internal consistency of the applied size categorization framework. Season correlated moderately with length (ρ = 0.537) and type (ρ = 0.508). Morphology, by contrast, showed no significant correlation with site (ρ = 0.039, ns) or season (ρ = −0.091, ns), as shown in the correlation matrix in Figure 6. This absence of a significant correlation is consistent

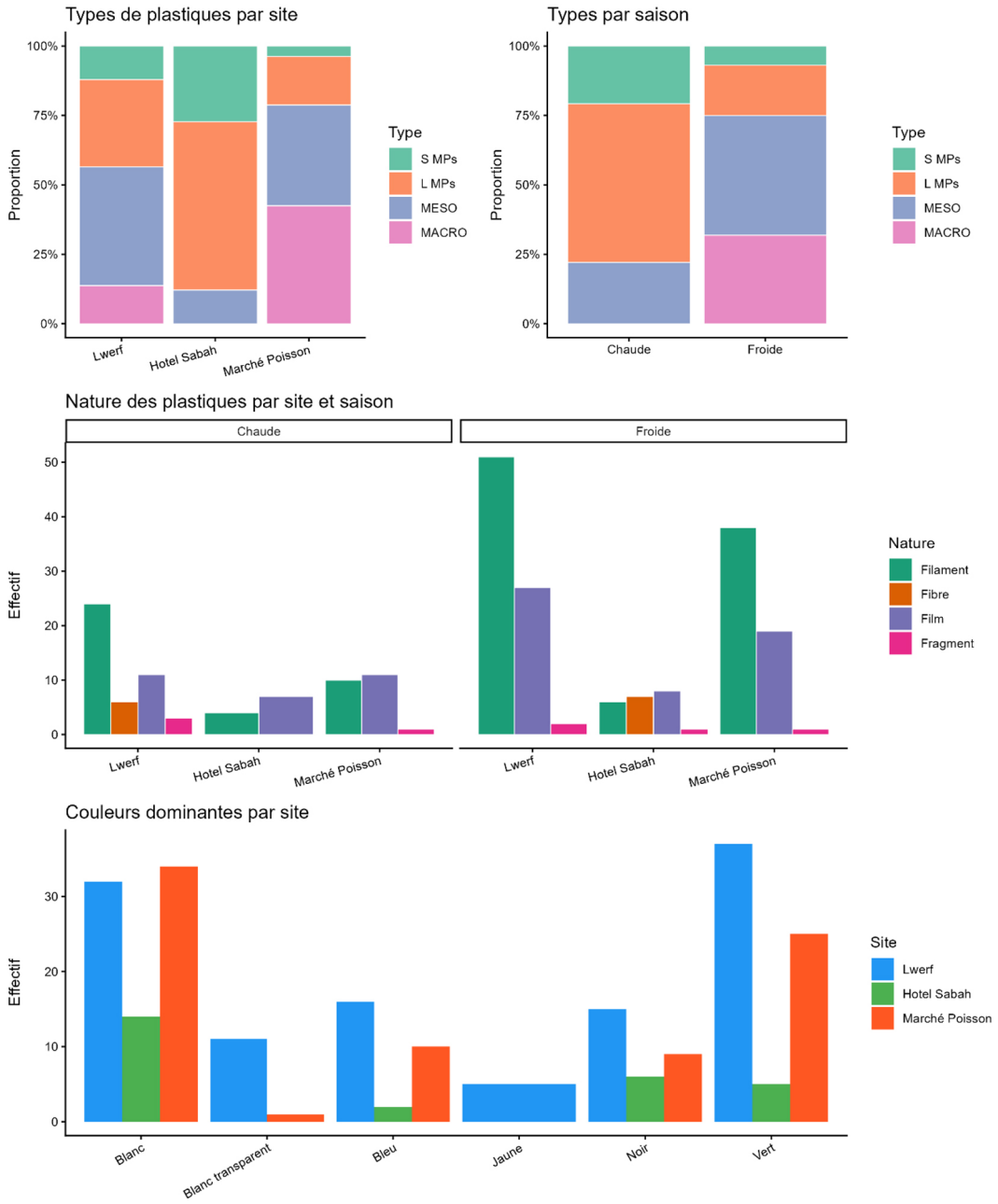

Figure 5. MP composition by type, morphology, and color. Top left: proportions of size types by site. Top right: proportions of size types by season. Middle row: morphological categories by site and season. Bottom: dominant colors (top six) by site. Stacked bar charts; percentages calculated within each group

with a relatively stable morphological fingerprint across sites and seasons; however, given the limited number of tow samples (n = 24, despite n = 237 particles), statistical power for detecting subtle compositional shifts is low and this observation should be interpreted as exploratory, requiring confirmation through a larger sampling design. All raw outputs supporting Section Spearman correlations – (full Spearman correlation matrix, p-values, R session information) are available in Annex S4.

Site-specific morphological signatures and morphology-based source hypotheses

Correspondence analysis on the morphology × site contingency table (Dim 1 = 92.7%) produced the clearest source discrimination in the entire dataset (Figures 7 and 8). Three distinct associations emerged: Hotel Sabah with fibers, Fish Market with films, Lwerf with filaments and fragments. We stress, in line with the reviewer's comment, that this is a

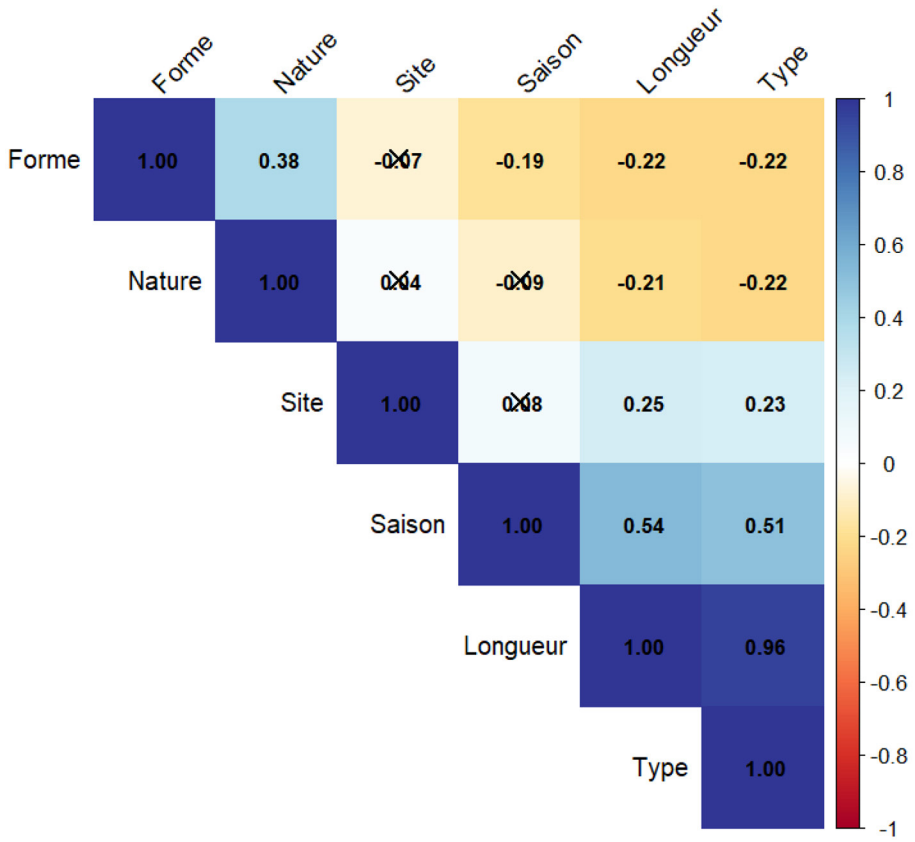

Figure 6. Spearman rank correlation matrix for all MP variables. Blue circles = positive correlations; red circles = negative correlations. Circle size proportional to |ρ|. Crosses mark non-significant correlations ($p > 0.05$)

morphology-based source hypothesis, not a fingerprint-based source identification. In the absence of FTIR/Raman polymer fingerprints and of source-apportionment tracers (e.g. additive signatures, isotopic markers), polyethylene/polypropylene cannot be confirmed, and the wastewater/fishing/tourism source pathways cannot be causally attributed. Throughout the following paragraphs we therefore use the formulation "compatible with" rather than "originating from", and the hydrodynamic/photodegradation/tourism mechanisms invoked below are presented as plausible drivers, not as directly measured forcings. Fibers observed at Hotel Sabah are morphologically compatible with potential domestic wastewater inputs carrying synthetic textile microfibers, although this interpretation remains hypothetical in the absence of polymer-specific confirmation. Hossain et al. (2025) recently estimated that fibrous MPs make up 49–70% of the total MP load in wastewater worldwide, originating largely from textile manufacturing and household washing of synthetic fabrics. The same pattern was reported in Senegalese coastal waters, where fibers dominated near urban centers due to untreated domestic discharges (Sonko et al., 2023). Off the Canary Islands, Huelbes et al. (2025) traced fiber contamination in invasive crab stomachs directly to nearby wastewater outfalls. Nouakchott's lack of advanced wastewater treatment makes this source pathway even more likely.

Films detected at Fish Market are morphologically compatible with degradation of single-use packaging materials associated with fish handling and retail activities, although polymer composition was not chemically verified. These thin films break apart easily under mechanical stress but keep their recognizable shape in surface waters close to the point of release (Figure 9).

Filaments detected at Lwerf may reflect degradation of fishing-related materials such as ropes, nets, and lines, although definitive attribution would require polymer-level confirmation. ALDFG has become a well-documented contributor to marine plastic pollution (Richardson et al., 2019), and Ramos et al. (2025) recently confirmed through combined laboratory, field, and survey work that braided polyethylene nets shed fibers and filaments once exposed to

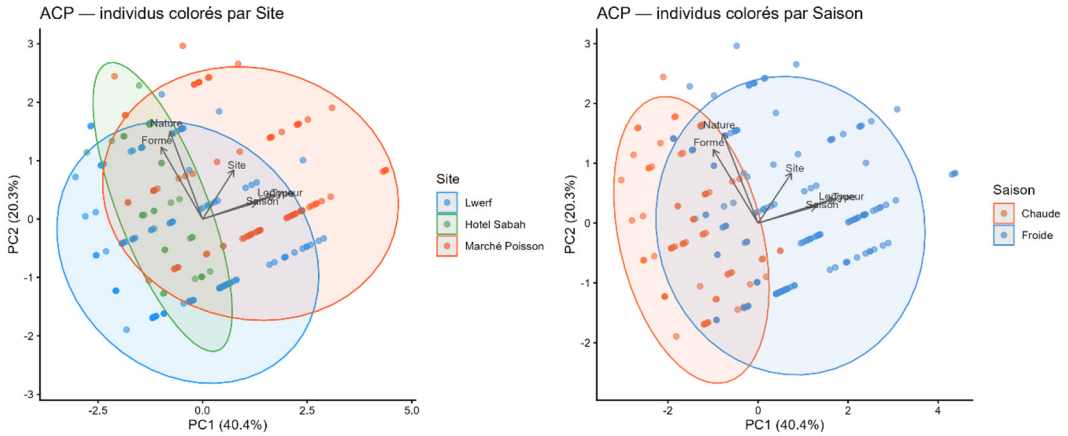

Figure 7. PCA biplot. Left: individual particles colored by site, with 95% convex-hull envelopes. Right: individuals colored by season. PC1 = 40.4%, PC2 = 20.3%. PC1 captures the size–season gradient; Fish Market clusters toward positive PC1 (large, cold-season particles) while Hotel Sabah forms a compact group in the upper-left quadrant (small, stable particles)

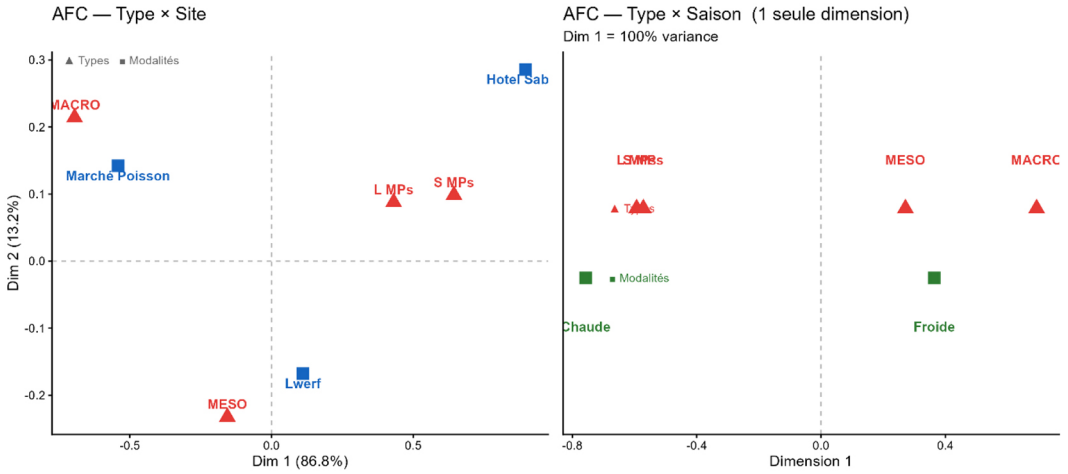

Figure 8. Correspondence analysis biplots. Left: Type × Site (2D; Dim 1 = 86.8% of inertia). Hotel Sabah associates with S MPs and L MPs (positive side), Lwerf with MESO (negative), Fish Market with MACRO (negative). Right: Type × Season (1D; 100% of inertia). Warm season groups with S MPs and L MPs; cold season with MESO and MACRO. Red triangles = MP types; blue squares = sites or seasons

environmental weathering. Given the intensity of fishing activity along the Mauritanian upwelling coast (FAO, 2021; ISSF, 2025), this source is expected to be substantial at Lwerf. The high color diversity at this site (H' = 1.814; Figure 10) reinforces the multi-source interpretation, since each pollution pathway contributes materials of distinct colors.

Multivariate structure: PERMANOVA and explained variance

PERMANOVA (Gower distance, 999 permutations) attributed approximately 40% of multivariate variance to site ($R^2 = 0.400$, $F = 176.8$, $p = 0.001$) and another 40% to season ($R^2 = 0.399$, $F = 352.9$, $p = 0.001$), for a combined total of 79.9% (Table 4). The site × season interaction was not significant ($p = 1.000$), meaning the two factors operate additively.

This unusually high explained variance should nevertheless be interpreted cautiously, as limited sample size and replication structure may contribute to inflation of multivariate effect estimates. Marsay et al. (2023) reported only 15–25% for location effects in Mediterranean MP communities, and Silva Barbosa et al. (2025) reported comparable proportions for spatial structure in a tropical urban estuary. The higher value here likely reflects two things: the sharp functional contrast

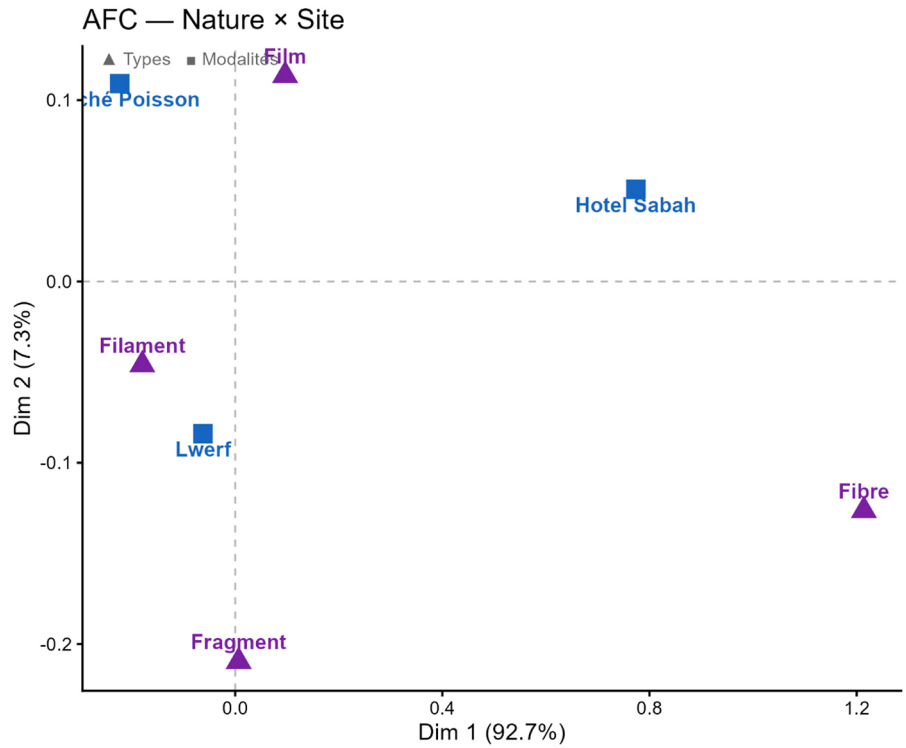

Figure 9. Correspondence analysis – morphology × site. Dim 1 = 92.7%, Dim 2 = 7.3%. Fibers associate with Hotel Sabah, films with Fish Market, filaments and fragments with Lwerf. Purple triangles = morphological categories; blue squares = sites. The near-total concentration of inertia on Dim 1 indicates a single dominant gradient of morphological differentiation

Table 4. PERMANOVA results (adonis2) for multivariate MP composition. Gower distance, 999 permutations. R^2 = proportion of variance explained. ** $p < 0.01$, ns = not significant

Factor	df	Sum of squares	R^2	Var. expl.	F	p-value	Sig.
Site	2	7.556	0.400	40.0%	176.8	0.001	**
Season	1	7.541	0.399	39.9%	352.9	0.001	**
Site × Season	2	—	—	—	—	1.000	ns

among our three sites (port vs. tourism vs. fishing) and the strong upwelling-driven seasonality of the eastern Atlantic, which creates a steeper environmental gradient than most tropical systems. It is also possible that the limited number of tow samples (n = 24) contributes to an overestimation of these effects; a larger sampling design would help confirm the robustness of these proportions.

The non-significant interaction term suggests that no statistically detectable site-specific seasonal effect was observed under the present sampling design. This is consistent with the hypothesis that the seasonal component is region-wide rather than site-specific, though future studies should directly test whether management strategies can indeed be applied uniformly across sites. PCA captured 60.7% of variance on two axes (PC1 = 40.4%, PC2 = 20.3%). PC1 tracked the size-season gradient; Fish Market clustered toward positive PC1 (large, cold-season particles) and Hotel Sabah toward the upper-left quadrant (small, stable particles; Figure 7). The CA on type × site captured 86.8% of inertia on Dimension 1, associating Hotel Sabah with S MPs/L MPs, Lwerf with MESO, and Fish Market with MACRO (Figure 8, left). The CA on type × season (1D, 100% inertia) placed the warm season with smaller particles and the cold season with larger ones (Figure 8, right). The full raw PERMANOVA output (adonis2 console output, permutation matrix, Gower distance matrix, betadisper dispersion test, PCA and CA input matrices with full eigenvalue tables) is available in Annex S4.

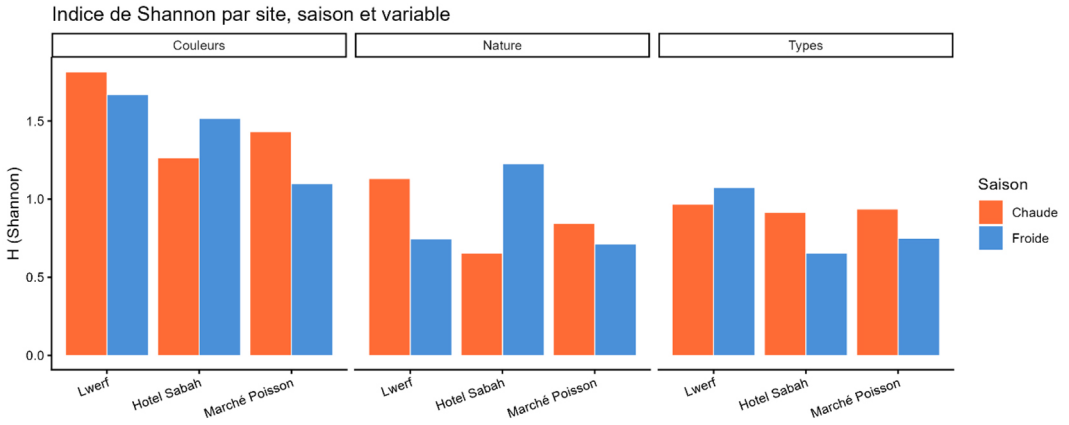

Figure 10. Shannon diversity index (H') for color, morphology, and size-type categories, broken down by site and season. Bar heights represent H' values. Lwerf consistently shows the highest diversity across all three classification schemes, while Hotel Sabah and Fish Market display lower, more specialized profiles

Shannon diversity and what it tells us about sources

Type diversity peaked at Lwerf during the cold season (H' = 1.075 [95% CI: 0.89–1.19], S = 4 types) and hit its minimum at Hotel Sabah during the cold season (H' = 0.655 [95% CI: 0.47–0.69], S = 2). Color diversity was highest at Lwerf (H' = 1.814 [95% CI: 1.36–1.99]). Pielou evenness reached its maximum at Hotel Sabah in the cold season (J = 0.946) and its minimum at Fish Market in the cold season (J = 0.683), where MACRO particles were heavily dominant (Figure 10). Bootstrap 95% confidence intervals (1.000 iterations, percentile method, package *boot*) were computed for all H' values and are shown as error bars in Figure 10. The full set of H' estimates with bootstrap CIs is reported in Table S3 (Annex S4) for the six site × season combinations and the three classification schemes (type, morphology, colour).

These diversity patterns complement the PERMANOVA and CA findings by capturing within-site heterogeneity. High diversity at Lwerf is consistent with contributions from multiple potential anthropogenic inputs, although diversity indices alone cannot definitively resolve pollution-source composition. Low diversity and high evenness at Hotel Sabah, by contrast, are compatible with a single dominant input – plausibly domestic fibres – although this remains a morphology-based hypothesis to be confirmed by polymer analysis. This kind of diversity-based source inference has been standard practice in macro-invertebrate ecology for decades but is still rare in MP research. Its application here demonstrates that diversity indices can flag a contrast between multi-source and single-source contamination regimes; it does not replace polymer identification, which remains required for definitive source attribution.

Methodological scope and limitations

Three analytical choices made in this study are not yet common in the MP literature and may prove useful for other researchers working with similar data: (i) reporting Cramér's V alongside chi-square p-values, which allows cross-variable comparison of association strength on a single metric; (ii) combining PERMANOVA, CA, and Shannon diversity in one framework, which captures between-group differences, variable-site associations, and within-group heterogeneity in a complementary way; and (iii) using Gower distance in PERMANOVA, which handles the mixed continuous-categorical structure of MP datasets more naturally than Euclidean or Bray-Curtis metrics (Anderson, 2017).

We acknowledge two key limitations. First, particles were not identified by polymer composition (FTIR or Raman spectroscopy). This means that the present study does not provide definitive confirmation of polymer type, and all source attributions are based on morphological evidence alone and should be interpreted as hypotheses requiring polymer-level verification. FTIR or Raman spectroscopy would have allowed definitive material confirmation and sharper source attribution, and should be integrated in future work. Second, quantitative abundance data (particles/m^3) could not be calculated because flow-meter readings were not available for every tow – a common constraint in

first-generation baseline studies from data-scarce regions. Both gaps should be addressed in follow-up work, which should also extend sampling to sediments and biota. Consequently, the present work focuses primarily on comparative morphological composition rather than absolute environmental concentration estimates. Beyond these two principal limitations, four additional methodological constraints should be borne in mind.

a) Polymer-fingerprint absence: morphological identification under stereomicroscopy is more prone to false positives than FTIR/Raman; we mitigated this risk by applying Hartmann et al. (2019) visual criteria and archiving the full image set in Annex S3, but a chemical subsample (≥ 10–15% of particles) by μ-FTIR or Raman is recommended for the follow-up campaign and will allow re-classification of the present dataset.
b) Sample size: 24 tow samples (4 transects × 3 sites × 2 seasons) is modest. While 237 particles provided enough power to detect large effects (η^2H, Cramér's V), it limits the power to detect small effects (such as the morphology–season relationship) and tends to inflate PERMANOVA R^2 values.
c) Pseudoreplication risk: multiple particles per tow are not fully independent observations; the present particle-level analysis describes patterns within this nested structure, and future studies should adopt mixed-effects / hierarchical models with the tow as a random factor.
d) Surface-water-only sampling: the dataset only captures the floating MP fraction (~ 15 cm depth); sediments, water-column, and biota compartments are not covered and may host complementary or contrasting MP signatures. Likewise, the ecological/mechanistic explanations invoked in Sections 3.6–3.10 (UV-driven photodegradation, current-driven redistribution, tourism-linked inputs, upwelling-driven hydrodynamic forcing) are plausible drivers consistent with our observations but were not directly measured in this study and should be regarded as hypotheses to be tested with dedicated process-oriented sampling (UV-A/UV-B dosimetry, ADCP current profiling, source-marker tracers). Full primary documentation supporting Sections Verification of statistical assumptions – methodological scope and limitations is provided in Annexes S1–S4 (raw particle inventory, raw test outputs, image archive, R scripts, R session information).

Management implications

The site-specific morphological signatures translate directly into management actions. At Hotel Sabah, where fibers dominate, the priority is domestic wastewater treatment and promotion of laundry lint filters. Laboratory tests of commercially available filters have shown they can reduce microfiber emissions from washing machines by up to 87% (McIlwraith et al., 2019). France has already mandated such filters on new washing machines, providing a regulatory model adaptable to Nouakchott. At Fish Market, the film signature calls for restrictions on single-use plastic packaging at the point of sale, paired with organized waste collection -approaches being tested under the WACA program (World Bank, 2023). At Lwerf, the filament pattern points to the need for fishing-gear recovery schemes and biodegradable net materials, in line with FAO (2021) and ISSF (2025) ALDFG guidelines.

The strong seasonal signal (r = 0.535; V = 0.525) also has operational value. Monitoring and beach cleanup efforts would gain efficiency if concentrated during or just before the cold season, when the larger, more ecotoxicologically concerning fractions (MESO, MACRO) build up the same fractions that carry the highest ingestion risk for marine megafauna and commercially important fish (Fossi et al., 2023).

CONCLUSIONS

This study establishes the first quantitative baseline for MP contamination in Nouakchott's coastal waters. PERMANOVA shows that site and season together account for roughly 80% of multivariate variance in MP composition (R^2_{site} = 0.400; R^2_{season} = 0.399; Table 4), with no significant interaction -the two factors operate independently and additively. In practice, where particles are found depends on the local source mix, while when they accumulate depends on region-wide oceanographic and climatic drivers.

Season exerts the stronger control over particle size (η^2_H = 0.282 vs. 0.223 for site; Table 2; Figure 4). Cold-season samples are dominated by mesoplastics and macroplastics, driven by reduced photodegradation and stronger hydrodynamic transport during upwelling.

Correspondence analysis revealed distinct morphology-based contamination patterns among sites that may reflect differences in dominant local anthropogenic activities, although polymer-level analyses would be required for definitive source attribution. Shannon color diversity confirms Lwerf as the most heterogeneous site (H' = 1.814; Figure 10), receiving simultaneous inputs from urban, fishing, and commercial activities, whereas Hotel Sabah and Fish Market show narrower contamination profiles.

Methodologically, the combination of Cramér's V, PERMANOVA, CA, and Shannon diversity within one framework proved well suited to the non-normal, mixed-variable structure of MP datasets (Table 3) and is readily transferable to other coastal settings where parametric assumptions do not hold.

These findings call for waste-management strategies in Nouakchott tailored to each site's dominant source and timed to the seasonal accumulation cycle. Monitoring and cleanup would gain efficiency if concentrated before or during the cold season, when larger, ecotoxicologically concerning fractions accumulate. The approach also provides a template applicable to other understudied West African coastlines. Overall, the present study should be considered a first morphology-based baseline assessment of microplastic contamination in Mauritanian coastal waters, providing exploratory evidence intended to guide future chemically validated investigations.Future work should prioritize polymer identification (FTIR/Raman spectroscopy) to enable definitive source attribution beyond morphological inference, alongside quantitative abundance estimates (particles/m³), and sampling of sediment and biota compartments.

REFERENCES

1. Alimi, O.S., Fadare, O.O., Okoffo, E.D., (2021). Microplastics in African ecosystems: current knowledge, abundance, associated contaminants, techniques, and research needs. *Sci. Total Environ. 755*, 142422. https://doi.org/10.1016/j.scitotenv.2020.142422
2. Anderson, M.J., (2017). *Permutational multivariate analysis of variance (PERMANOVA)*. In: Wiley StatsRef: Statistics Reference Online. Wiley. https://doi.org/10.1002/9781118445112.stat07841
3. Andrady, A.L., (2011). Microplastics in the marine environment. *Mar. Pollut. Bull. 62*, 1596–1605. https://doi.org/10.1016/j.marpolbul.2011.05.030
4. Aragaw, T.A., (2021). Microplastics in the coastal environment of Ghana: extent, current knowledge, and gaps. *Reg. Stud. Mar. Sci. 44*, 101745. https://doi.org/10.1016/j.rsma.2021.101745
5. Bao, M., Xiang, X., Huang, J., Kong, L., Wu, J., Cheng, S., (2023). Microplastics in the atmosphere and water bodies of coastal agglomerations: a mini-review. *Int. J. Environ. Res. Public Health 20*, 2466. https://doi.org/10.3390/ijerph20032466
6. Bergmann, M., Mützel, S., Primpke, S., Tekman, M.B., Trachsel, J., Gerdts, G., (2019). White and wonderful? Microplastics prevail in snow from the Alps to the Arctic. *Sci. Adv. 5, eaax1157*. https://doi.org/10.1126/sciadv.aax1157
7. Boucher, J., Friot, D., (2017). Primary microplastics in the oceans: A global evaluation of sources. *IUCN, Gland, Switzerland.* https://doi.org/10.2305/IUCN.CH.2017.01.en
8. Browne, M.A., Crump, P., Niven, S.J., Teuten, E., Tonkin, A., Galloway, T., Thompson, R., (2011). Accumulation of microplastic on shorelines worldwide: sources and sinks. *Environ. Sci. Technol. 45*, 9175–9179. https://doi.org/10.1021/es201811s
9. Chukwuka, A.V., Adegboyegun, A.D., Oluwale, F.V., Oni, A.A., Omogbemi, E.D., Adeogun, A.O., (2024). Microplastic dynamics and risk projections in West African coastal areas: developing a vulnerability index, adverse ecological pathways, and mitigation framework using remote-sensed oceanographic profiles. Sci. Total Environ. 953, 175963. https://doi.org/10.1016/j.scitotenv.2024.175963
10. Cohen, J., (1988). *Statistical Power Analysis for the Behavioral Sciences, 2nd ed.* Lawrence Erlbaum Associates, Hillsdale. https://doi.org/10.4324/9780203771587
11. Cole, M., Lindeque, P., Halsband, C., Galloway, T.S., (2011). Microplastics as contaminants in the marine environment: a review. *Mar. Pollut. Bull. 62*, 2588–2597. https://doi.org/10.1016/j.marpolbul.2012.10.013
12. Cramér, H., (1946). *Mathematical Methods of Statistics*. Princeton University Press, Princeton. https://doi.org/10.1515/9781400883868
13. Enders, K., Lenz, R., Stedmon, C.A., Nielsen, T.G., (2015). Abundance, size and polymer composition of marine microplastics ≥ 10 μm in the Atlantic Ocean. *Mar. Pollut. Bull. 151*, 110858. https://doi.org/10.1016/j.marpolbul.2019.110858
14. FAO, (2021). *Assessment and monitoring of abandoned, lost, or discarded fishing gear*. FAO Technical Paper No. 668. Rome. https://doi.org/10.4060/cb5000en
15. Fossi, M.C., Baini, M., Panti, C., Baulch, S., (2023). Microplastics in Mediterranean biota: updated

review with emphasis on cetacean ingestion. *Mar. Pollut. Bull. 189*, 114775. https://doi.org/10.1016/j.marpolbul.2023.114775

16. GESAMP, (2015). *Sources, fate and effects of microplastics in the marine environment: a global assessment.* GESAMP Reports and Studies No. 90. IMO/FAO/UNESCO-IOC/UNIDO/WMO/IAEA/UN/UNEP/UNDP.
17. Gilman, E., Musyl, M., Suuronen, P., et al., (2021). Highest risk abandoned, lost and discarded fishing gear. *Sci. Rep. 11*, 7195. https://doi.org/10.1038/s41598-021-86123-3
18. Hartmann, N.B., Hüffer, T., Thompson, R.C., et al., (2019). Are we speaking the same language? Recommendations for a definition and categorization framework for plastic debris. *Environ. Sci. Technol. 53*, 1039–1047. https://doi.org/10.1021/acs.est.8b05297
19. Hossain, M.I., Zhang, Y., Haque, A.N.M.A., Naebe, M., (2025). Fibrous microplastics release from textile production phases: a brief review. *Materials 18*, 2513. https://doi.org/10.3390/ma18112513
20. Isobe, A., Iwasaki, S., Uchida, K., Tokai, T., (2019). Abundance of non-conservative microplastics in the upper ocean from 1957 to 2066. *Nat. Commun. 10*, 417. https://doi.org/10.1038/s41467-019-08316-9
21. ISSF, (2025). Guidelines for Developing Plans of Action on Managing Abandoned, Lost and Discarded Fishing Gear. *ISSF Technical Report 2025-07*. International Seafood Sustainability Foundation, Washington DC.
22. Jambeck, J.R., Geyer, R., Wilcox, C., et al., (2015). Plastic waste inputs from land into the ocean. *Science 347*, 768–771. https://doi.org/10.1126/science.1260352
23. Lebreton, L.C.M., van der Zwet, J., Damsteeg, J.W., et al., (2017). River plastic emissions to the world's oceans. *Nat. Commun. 8*, 15611. https://doi.org/10.1038/ncomms15611
24. Li, J., Liu, H., Chen, J.P., (2018). Microplastics in freshwater systems: a review on occurrence, environmental effects, and methods for detection. *Water Res. 137*, 362–374. https://doi.org/10.1016/j.watres.2018.01.015
25. Marsay, K.S., Ambrosino, A.C., Koucherov, Y., et al., (2023). Geographical and seasonal effects on marine microplastic composition. *Front. Microbiol. 14*, 1089926. https://doi.org/10.3389/fmicb.2023.1089926
26. McIlwraith, H.K., Lin, J., Erdle, L.M., et al., (2019). Capturing microfibers — marketed technologies reduce microfiber emissions from washing machines. *Mar. Pollut. Bull. 139*, 40–45. https://doi.org/10.1016/j.marpolbul.2018.12.012
27. Mint Sidi Mohamed, F., (2017). *Gestion des déchets solides à Nouakchott: diagnostic et perspectives.* Thesis, Université de Nouakchott.
28. Okeke, S.E., Olagbaju, A.O., Okoye, O.C., et al., (2022). Microplastic burden in Africa: A review. *Chem. Eng. J. Adv. 12*, 100402. https://doi.org/10.1016/j.ceja.2022.100402
29. Pappoe, C., Armah, F.A., Kwakye, P.K., Afriyie-Kraft, L., Adomako, D., (2022). Microplastics in coastal and marine fish from the Greater Accra Region, Ghana. Mar. *Pollut. Bull. 181*, 113862. https://doi.org/10.1016/j.marpolbul.2022.113862
30. PlasticsEurope, (2024). *Plastics — The Fast Facts 2024*. PlasticsEurope, Brussels. Available at: https://plasticseurope.org/knowledge-hub/plastics-the-fast-facts-2024/
31. Prata, J.C., da Costa, J.P., Duarte, A.C., Rocha-Santos, T., (2019). Methods for sampling and detection of microplastics in water and sediment: a critical review. *TrAC Trends Anal. Chem. 110*, 150–159. https://doi.org/10.1016/j.trac.2018.10.029
32. Ramos, S., Espincho, F., Rodrigues, S.M., Pereira, R., Silva, D., Rivoira, L., Perdigão, R., Almeida, C.M.R., 2025. An integrated approach to assessing the potential of plastic fishing gear to release microplastics. *Water* 17, 1439. https://doi.org/10.3390/w17101439
33. Richardson, K., Hardesty, B.D., Wilcox, C., (2019). Estimates of fishing gear loss rates at a global scale. *Fish Fish. 23*, 1115–1130. https://doi.org/10.1111/faf.12677
34. Rochman, C.M., Brookson, C., Bikker, J., et al., (2019). Rethinking microplastics as a diverse contaminant suite. *Environ. Toxicol. Chem. 38*, 703–711. https://doi.org/10.1002/etc.4371
35. Shannon, C.E., (1948). A mathematical theory of communication. *Bell Syst. Tech. J. 27*, 379–423. https://doi.org/10.1002/j.1538-7305.1948.tb01338.x
36. Silva Barbosa, F.C., Alves, R.S., Carneiro dos Santos, V.M., et al., (2025). Spatio-temporal dynamics of microplastic pollution in surface waters of a tropical urban estuary (Northeastern Brazil). *Reg. Stud. Mar. Sci. 79*, 103882. https://doi.org/10.1016/j.rsma.2025.103882
37. Sonko, A., Brehmer, P., Constantin de Magny, G., Le Pennec, G., Sambe Ba, B., Diankha, O., Fall, M., Linossier, I., Henry, M., N'Diaye, I., Faye, S., Kande, Y., Galgani, F., 2023. Pollution assessment around a big city in West Africa reveals high concentrations of microplastics and microbiologic contamination. *Reg. Stud. Mar. Sci.* 59, 102755. https://doi.org/10.1016/j.rsma.2022.102755
38. Thompson, R.C., Olsen, Y., Mitchell, R.P., et al., (2004). Lost at sea: where is all the plastic? *Science 304*, 838. https://doi.org/10.1126/science.1094559

39. Thompson, R.C., Courtene-Jones, W., Boucher, J., Pahl, S., Raubenheimer, K., Koelmans, A.A., (2024). Twenty years of microplastic pollution research — what have we learned? *Science 386*, 6720. https://doi.org/10.1126/science.adp5765
40. Valdés, L., Déniz-González, I. (Eds.), (2015). *Oceanographic and Biological Features of the Canary Current Large Marine Ecosystem*. IOC Technical Series No. 115. IOC-UNESCO, Paris.
41. Woodall, L.C., Sanchez-Vidal, A., Canals, M., et al., (2014). The deep sea is a major sink for microplastic debris. *R. Soc. Open Sci. 1*, 140317. https://doi.org/10.1098/rsos.140317
42. World Bank, (2023). West Africa Coastal Areas Management Program (WACA): Plastic Pollution Assessment. World Bank Group, Washington DC. Available at: https://www.worldbank.org/en/programs/west-africa-coastal-areas-management-program